ChemPubSoc Europe

DOI: 10.1002/chem.201804012

CHEMISTRY A European Journal Communication

Methane Storage

Incorporating Heavy Alkanes in Metal–Organic Frameworks for Optimizing Adsorbed Natural Gas Capacity

Yu Fang[+],[a] Sayan Banerjee[+],[a] Elizabeth A. Joseph[+],[a] Gregory S. Day,[a] Mathieu Bosch,[a] Jialuo Li,[a] Qi Wang,[a] Hannah Drake,[a] Osman K. Ozdemir,[a, b] Jason M. Ornstein,[b] Ye Wang,[c] Tong-Bu Lu,[c] and Hong-Cai Zhou*[a, d]

Abstract: Metal–organic frameworks (MOFs) as methane adsorbents are highly promising materials for applications such as methane-powered vehicles, flare gas capture, and field natural gas separation. Pre- and post-synthetic modification of MOFs have been known to help improve both the overall methane uptake as well as the working capacity. Here, a post-synthetic modification strategy to non-covalently modify MOF adsorbents for the enhancement of the natural gas uptake for the MOF material is introduced. In this study, PCN-250 adsorbents were doped with C_{10} alkane and C_{14} fatty acid and their impact on the methane uptake capabilities was investigated. It was found that even trace amounts of heavy hydrocarbons could considerably enhance the raw methane uptake of the MOF while still being regenerable. The doped hydrocarbons are presumably located at the mesoporous defects of PCN-250, thus optimizing the framework–methane interactions. These findings reveal a general approach that can be used to modify the MOF absorbents, improving their ability to be sustainable and renewable natural gas adsorption platforms.

Natural gas, the principal ingredient of which is methane, can either be directly used as a fuel or processed into other energy resources.[1] Many energy-intensive solutions have been proposed to capture, store, and transport natural gas into the US energy infrastructure.[2] For example, natural gas can be successfully compressed to higher pressures up to 250 bar (3,600 psi), which is commonly referred to as compressed natural gas (CNG). It can also be liquefied at the temperatures less than −160 °C, producing liquefied natural gas (LNG). These century-old technologies are known to improve the energy density of natural gas, to 9.2 MJ L^{-1} for CNG or 22.2 MJ L^{-1} for LNG respectively, but they are subsequently downgraded by about 30% volumetrically to account for their real cylindrical containment requirements.[3] In addition, both applications have intensive energy demands, creating critical cost issues. These issues have resulted in failure to fully utilize America's natural gas reserves.

Adsorbed natural gas (ANG) is an increasingly important method of improving natural gas storage.[4,5] In the past few decades, a variety of candidate absorbents, containing high surface areas, controlled pore diameters, and moderate binding energies, have been developed for research.[6] As a precisely tunable porous material, metal–organic frameworks (MOFs) have attracted great interest recently with their potential to boost ANG technologies.[7] Theoretical works suggested a conceptual MOF, IRMOF-993, could have a volumetric methane storage capacity well above activated carbon.[8] However, the MOFs in the study suffers from low chemical stability, especially in the presence of trace natural gas pollutants like hydrogen sulfide or water vapor.[9,10] Alternatively, an iron cluster-based MOF, PCN-250, is a radical departure from previously reported ANG MOFs due to its considerably higher stability. It is stable in boiling water as well as a wide range of pH conditions, maintaining its crystal structure and surface area. Moreover, PCN-250 exhibits a total reported methane storage capacity of 180 *v*(STP)/*v*, exhibiting a flat heat of adsorption curve, while also being capable of low-cost production.[11]

Here, we provide a post-synthetic treatment of PCN-250, aiming to obtain an enhanced, regenerable methane storage absorbent. The addition of a small portion of high boiling point alkanes into natural gas to increase the compression and/or refrigeration storage have been used for CNG and LNG for many years.[12,13] The alkanes not only increased the boiling point of the liquefied methane but also dissolved the hydrophobic methane through hydrophobic interactions.[14] Inspired by this idea, we incorporated C_{10} and C_{14} hydrocarbons into the pores of PCN-250 as a method of improving the ANG concept. We have dubbed the combination of methane absorption in high alkanes at high pressures, and its adsorption on

[a] *Dr. Y. Fang,[+] S. Banerjee,[+] E. A. Joseph,[+] G. S. Day, Dr. M. Bosch, J. Li, Q. Wang, H. Drake, O. K. Ozdemir, Prof. Dr. H.-C. Zhou*
Department of Chemistry, Texas A&M University
College Station, Texas 77843-3255 (USA)
E-mail: zhou@chem.tamu.edu

[b] *O. K. Ozdemir, J. M. Ornstein*
framergy Inc, 800 Raymond Stotzer Parkway, 2011
College Station, Texas 77843-3255 (USA)

[c] *Y. Wang, Prof. T.-B. Lu*
Institute of New Energy Materials & Low Carbon Technology
School of Material Science & Engineering
Tianjin University of Technology, Tianjin, 300384 (P. R. China)

[d] *Prof. Dr. H.-C. Zhou*
Department of Materials Science and Engineering
Texas A&M University, College Station, Texas 77843-3003 (USA)

[+] *These authors contributed equally to this work.*

Supporting information and the ORCID identification number(s) for the author(s) of this article can be found under: https://doi.org/10.1002/chem.201804012.

the surface/pores of a porous material, HAANG (High Alkane Adsorbed Natural Gas).[15] The doped system allows for a higher volume of methane to be stored as compared to the unmodified adsorbent at a given pressure. Most of the high alkane is also retained in and on the adsorbent through many working cycles of adsorption and desorption. This two-phase process, containing both liquid and vapor, can be achieved at suitable pressures (30–100 bar) and temperatures (260–323 K) for ANG technology.

To realize the HAANG process, an apparatus was designed and constructed for direct volumetric measurement of methane uptake and delivery, as shown in Figure 1 A and B (also see Figures S1 and S2, Supporting Information). The methane gas was first transported from the gas tank (① in Figure 1 A) to the charger unit ⑤. Then, the PCN-250 adsorbent (1 gram) was loaded into a test cell, ⑧. By controlling the valves (④, ⑥ and ⑦), methane gas can be transported to the test cell and adsorbed by PCN-250. Due to the presence of a pressure transducer (P/T) on the bottom of the charging unit, the final pressure (P_{fin}) can also be recorded. The initial pressure subjected to the methane supply inlet was assigned as P_{ini} (960 psi). By comparing the P_{ini} and P_{fin}, the adsorbed gas volume can be measured by the ΔP ($P_{ini}-P_{fin}$). Furthermore, the adsorbed gas in the test cell was discharged from the system and released into an airbag (1 L). A flow of atmospheric air was then injected into the airbag until it was full (1 L) to dilute the methane gas. A gas syringe was then used to inject 10 mL of the gas mixture into a gas chromatography-flame ionized detector (GC-FID). Due to the deliverable methane being different for every experiment and the total volume of the airbag is a constant (1 L), the 10 mL in the syringe contains different amounts of methane. The injected methane gas was quantified by the integration area of the GC data. The integration area can represent the different ratio of deliverable methane in the air bag, thus the variation of deliverable methane can be analyzed. By using this system, it was found that PCN-250 can absorb and deliver an almost equal amount of methane gas repeatedly.

The methane uptake capacity of the alkane-doped PCN-250 samples (defined as Decane@PCN-250) were also measured with their methane uptake properties according to the above procedure. A sample of 1 gram of PCN-250 was filled in the test cell and fully activated under vacuum at 160 °C. Then the test cell was taken into an inert atmosphere (glove box) and 60 μL of *n*-decane was injected. After standing for 20 min, the test cell was sealed with 2 μm VCR gasket for the following gas test. Methane gas at 960 psi (66.2 bar) pressure was stored in the charger unit and then injected into the test cell. The pressure drop ΔP for the PCN-250 sample was 275 psi, which could be translated into adsorbed methane. Surprisingly, when PCN-250 was doped with *n*-decane, we found there was a dramatic increase of 21.8% for the ΔP (335 vs. 275 psi, Figure 1 C). This suggests that *n*-decane-doped PCN-250 has a storage capacity 21.8% greater than that of pristine PCN-250. Figure 1 D shows a GC chromatogram comparing deliverable methane from PCN-250 at atmospheric pressure in the presence and absence of the doping agent (*n*-decane). Similarly, when PCN-250 was doped with *n*-decane, an 18.0% increase in the integrated

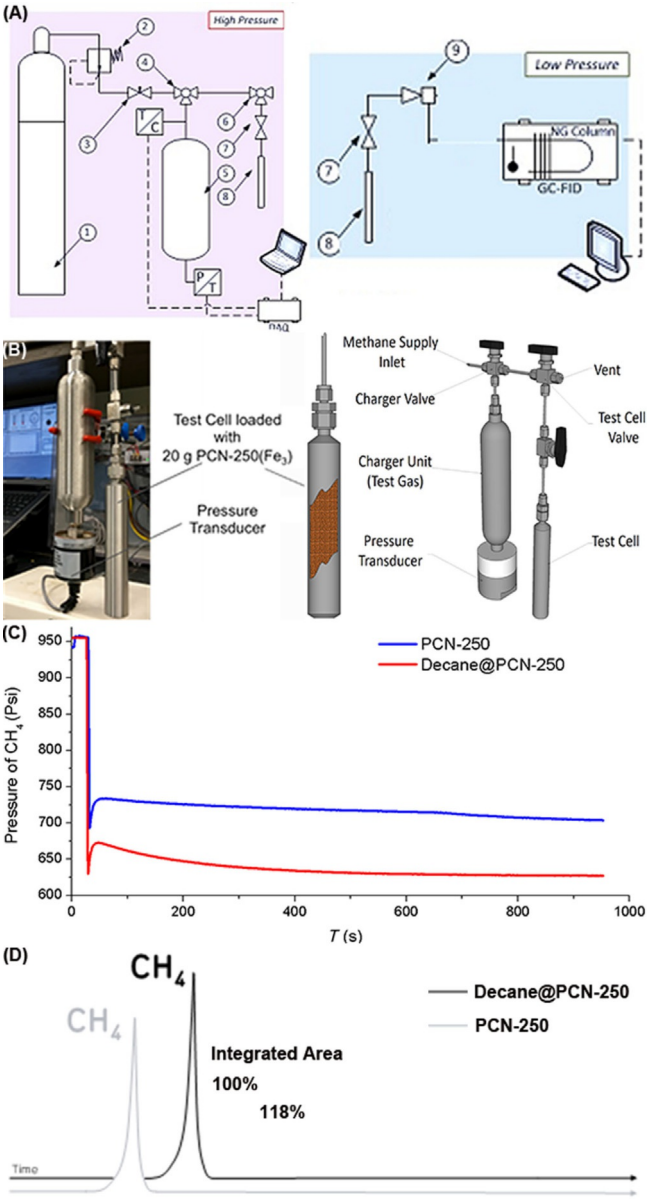

Figure 1. (A) Scheme of real-time gas adsorption/desorption monitoring station. (①: Test gas; ②: Pressure regulator; ③: Needle valve; ④: 3-way valve; ⑤: Test canister; ⑥: 3-way valve; ⑦: Ball valve; ⑧: Sorbent column; ⑨: Ejector/Injector; T/V: Thermocouple; P/T: Pressure Transmitter; GC: Gas Chromatograph; FID: Flame Ionization Detector). (B) A detailed demonstration of the charger unit, sample cell (⑧) and connections (④, ⑥, and ⑦) monitoring station system. (C) Real-time monitoring of pressure drop of PCN-250 and PCN-250 doped with n-decane. (D) The GC-FID chromatogram shows the deliverable methane from PCN-250 and PCN-250 doped with n-decane.

area of the methane peak was observed. The pressure drop and GC results demonstrated an increase in total volumetric methane uptake of about 18% alongside the full desorption of methane, with the *n*-decane remaining in the PCN-250 adsorbent (not detectable by GC). It should be noted that the *n*-alkane loading was quite low (60 μL per 1 gram of adsorbent), accounting for 4.4 wt% of the MOF. When switched to a larger test tube filled with 20 gram of absorbents, a similar increase in methane uptake was observed. Not only PCN-250 but also

other microporous and mesoporous MOFs were found to have a similar increase in methane uptake when doped with different amounts and species of hydrocarbons (Figures S4–S10, Supporting Information). In addition, increasing the loading of *n*-decane with the MOF tended to result in decreasing methane storage capacity (Figures S11 and S12, Supporting Information). We assume that too much *n*-decane would block the entrance of methane, thus inducing a decrease of methane uptake. Further screening of doping agents and engineering of the MOF–dopant interactions are needed to understand the system and demonstrate it as a proof-of-concept.

Considering that *n*-decane (van der Waals diameter ~14 Å) is too large to be accommodated within the cavity of PCN-250 (pore size 8 Å), we hypothesized that it could be located within the mesoporous defects of the MOF. Thus, we introduced mesoporous defects into PCN-250 by Soxhlet treatment, to create mesoporous PCN-250 samples.[16] The PCN-250 sample prepared according to reported literature is defined as Micro-PCN-250. The Soxhlet treatment sample, Meso-PCN-250, maintained the same crystalline morphology (Figure S13, Supporting Information) as Micro-PCN-250 (Figure 2A and C). However, high-resolution scanning electron microscopy (SEM) imaging clearly revealed that the mesoporous defects (about 3–5 nm) were generated at the surface of Meso-PCN-250 (Figure 2B and D). The total N_2 uptake capacity of Meso-PCN-250 (398 $cm^3 g^{-1}$ STP) is largely similar to Micro-PCN-250 (405 $cm^3 g^{-1}$ STP). Notably, the N_2 adsorption-desorption isothermal (Figure 2E and F) at 77 K clearly displays a type-IV isothermal with hysteresis loops characteristic of large constricted mesopores for Meso-PCN-250, providing evidence for Soxhlet-induced mesopores within the framework. The pore-size distribution (Figure 2H), as determined by the Barrett–Joyner–Halenda (BJH) desorption model, unambiguously shows that Meso-PCN-250 has ordered 3.8 nm mesopores, whereas Micro-PCN-250 does not (Figure 2G). By comparing the DFT-calculated pore volumes of the two samples, it suggests that the micropore volume decreased from 0.285 to 0.186 $cm^3 g^{-1}$·Å after mesopores were introduced to the PCN-250 samples (Figures S16 and S17, Supporting Information). The high-pressure methane uptake of both PCN-250 adsorbents was measured at 298 K using a Micromeritics HPVA-II (Figures 2I and J). The Meso-PCN-250 has a methane uptake of 142 $cm^3 cm^{-3}$ at 65 bar, 11.8% lower than Micro-PCN-250 (161 $cm^3 cm^{-3}$). It is well-known that mesoporous MOFs tend to have poor methane storage capabilities due to the large pore openings not being optimized for binding methane molecules.[17] From the above characterization, we realized that Meso-PCN-250 maintains similar crystallinity and gas adsorption performance to Micro-PCN-250. However, Meso-PCN-250 exhibited a distinct pore-size distribution. The ordered and uniform mesopores of Meso-PCN-250 make it a suitable candidate for the investigation of hydrocarbon loading in PCN-250.

As the loaded alkanes investigated for the phenomenon tend to be in the gaseous or liquid phase and are easily desorbed, it is difficult to determine the actual loading within the MOF during tests. To prevent this ease of desorption, we opted to investigate fatty acid incorporation into MOFs. Considering that fatty acids are capable of coordinating with the metal cluster of the MOFs, they will have stronger binding to the MOF frameworks. Doped samples of *n*-decane and myristic acid, Decane@Meso-PCN-250 (4.4 wt% loaded) and Myristic@-Meso-PCN-250 (50 wt% loaded), were prepared accordingly. A PXRD spectrum of the doped absorbents showed a very similar pattern to that of as-synthesized PCN-250 and the simulated pattern (Figure 3A). The IR (infrared) spectrum (Figure 3B) of Myristic@Meso-PCN-250 shows a representative peak for myristic acid at 2800–2900 nm, indicative of successful binding of myristic acid to the MOF framework (Figures S20–S22, Supporting Information).[18] As seen in Figure 3C, the thermal stability of samples before and after doping was analyzed by thermal gravity analysis (TGA). The TGA curve of Meso-PCN-250 displays a mass loss of 5.6% below 100 °C, likely resulting from the removal of methanol from the framework. From 100–400 °C, the mass loss of Meso-PCN-250 is 17.0% corresponding

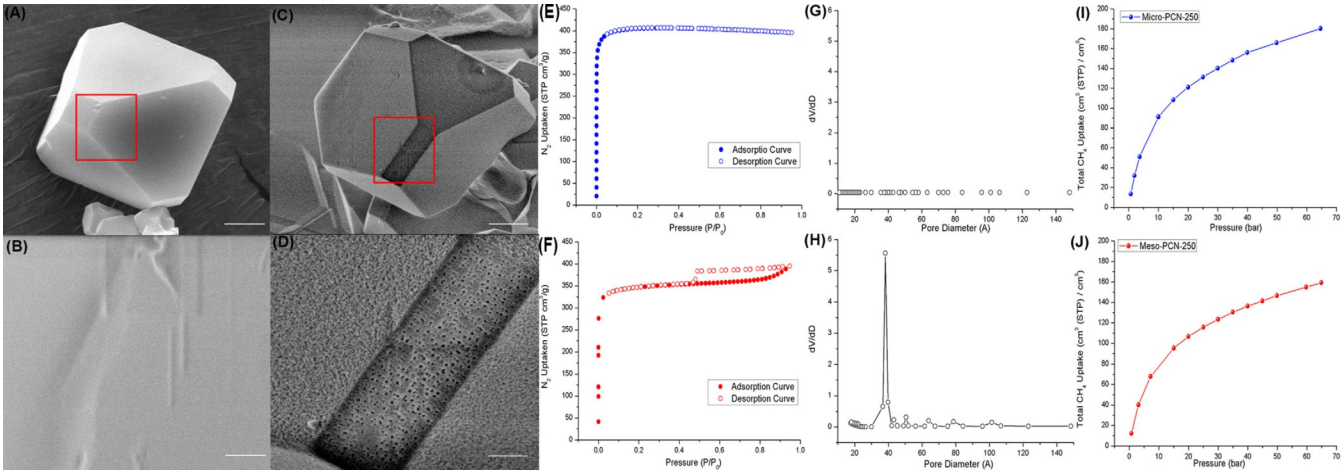

Figure 2. Characterization of Micro-PCN-250 and Meso-PCN-250. SEM images of (A) Micro-PCN-250 and (C) Meso-PCN-250. (B, D) Enlarged SEM images of the red reticular zone in (A) and (C). N_2 isotherm of (E) Micro-PCN-250 and (F) Meso-PCN-250. BJH Desorption pore size distribution of (G) Micro-PCN-250 and (H) Meso-PCN-250 (only the mesoporous region is shown). High-pressure methane uptake of (I) Micro-PCN-250 and (J) Meso-PCN-250. Scale bar for (A) and (B): 1 μm. Scale bar for (C) and (D): 200 nm.

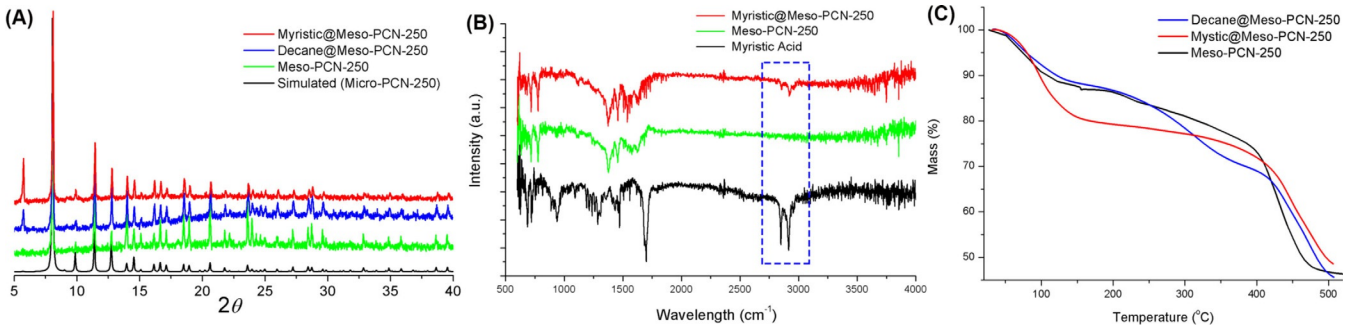

Figure 3. (A) Powder XRD pattern of Micro-PCN-250, Meso-PCN-250, Decane@Meso-PCN-250 and Myristic@Meso-PCN-250. (B) FT-IR spectrum of Meso-PCN-250 and Myrstic@Meso-PCN-250, and compared with Myristic Acid authentic sample. (C) TGA curve of Meso-PCN-250, Decane@Meso-PCN-250 and Myristic@-Meso-PCN-250.

to the loss of residual guest DMF molecules. The Decane@Meso-PCN-250 sample demonstrated a similar TGA curve, but with one more weight loss step (12.1%) starting from 220 °C, which resulted from the loss of decane (boiling point of 174 °C). However, the TGA of Myristic@Meso-PCN-250 exhibited major differences when compared to the above two samples in TGA. Below 150 °C, there is a significant mass loss of 19.2%, corresponding to the loss of methanol used in the loading of myristic acid (boiling point of 326 °C). In the range of 150–400 °C, the mass loss of Myristic@Meso-PCN-250 is only 7.3%, which is the smallest of the three compared samples. This showcases the relatively slow desorption of myristic acid as compared to *n*-decane and DMF. There is also a slight shift in framework decomposition temperature in the Myristic@Meso-PCN-250, from 400 °C to 410 °C. This shift suggests that the myristic acid attached to the MOF increases the thermal stability of the structure. After loading *n*-decane or myristic acid, the N_2 uptake of Meso-PCN-250 was considerably decreased (Figures S23 and S24, Supporting Information).

After doping with *n*-decane and myristic acid, both PCN-250 adsorbents were measured for high-pressure methane uptake at 298 K using the HPVA-II from Micromeritics (Figure 4A and B). The two doping reagents, *n*-decane, and myristic acid have minimal volumetric methane uptakes in the absence of the framework at 65 bar (10 $cm^3 cm^{-3}$ *v/v*). When Micro-PCN-250 was doped with *n*-decane and myristic acid, a decrease in methane uptake at 65 bar was observed (132 and 121 $cm^3 cm^{-3}$ *v/v*, respectively). Our simulation data also show the same trend as the experimental data (Figures S25 and S26, Supporting Information). In contrast, when Meso-PCN-250 was doped with *n*-decane, the methane uptake at 65 bar improved from 142 to 203 $cm^3 cm^{-3}$ *v/v*, which is a 43.0% increase compared to pristine Meso-PCN-250 (Figure 4A). When compared to the pristine Micro-PCN-250, the increased value is 26.1%, which is comparable to the 18% increase for deliverable methane [characterized by GC-FID (Figure 1D)]. In addition, the working capacity (5–65 bar) of Decane@Meso-PCN-250 was also elevated, reaching 159 compared to 110 $cm^3 cm^{-3}$ *v/v* for Micro-PCN-250. Myristic@Meso-PCN-250 can reach a total methane uptake capacity of 173 $cm^3 cm^{-3}$ *v/v* at 65 bar (Figure 4B), and 192 $cm^3 cm^{-3}$ *v/v* at 95 bar (Figure S28, Supporting Information). To the best of our knowledge, the 192–203 $cm^3 cm^{-3}$ *v/v* values represent record-high methane uptake of mesoporous PCN-250 adsorbents reported so far.[11,19] It was also noted that the methane uptake increased faster for *n*-decane than that for myristic-acid-doped samples when increasing the pressure (Figure 4C and D). This can likely be ascribed to the stronger interactions between methane and high alkanes such as *n*-decane.[20]

Although *n*-decane doping has better methane adsorption performance than myristic acid doping, the recyclability follows the reverse trend (Figure 4E and F). After three cycles, the performance of *n*-decane-doped samples was reduced to 50% of the initial cycle. Due to the lack of strong interactions between *n*-decane and the MOF, it is difficult to prevent the *n*-decane from leaching from the framework during the regeneration process, which included vacuum-assisted heating at 180 °C. After three cycles, the subsequent two cycles maintained a performance that was 45% that of the original. In contrast, myristic-acid-doped Meso-PCN-250 showed consistent performance even after three cycles. As expected, the carboxylic acid moieties of the fatty acid can bind to the metal cluster of the MOF adsorbent, reducing the loss of dopant during the desorption process.[21] The weight of myristic acid doped Meso-PCN-250 for each cycle was also measured, and no weight loss was found. This strongly indicated the retention of fatty acid within the framework throughout the gas storage cycle.

According to the results obtained above, the proposed mechanism of the enhanced methane uptake by long chain hydrocarbon doped PCN-250 is illustrated in Scheme 1. Through Soxhlet treatment, defects were created in the microporous PCN-250, yielding mesoporous PCN-250. Considering that mesopores have no significant interactions with small molecules, such as methane, methane uptake of undoped mesoporous PCN-250 was lower than that of undoped microporous PCN-250. In contrast, myristic acid strongly binds to the open metal sites of PCN-250, with long alkane chains located in the mesopores. By taking advantage of hydrophobic interactions and efficient space partition, methane molecules were packed into the mesopores, resulting in enhanced uptake capability. Although there are several pre- or post-synthetic

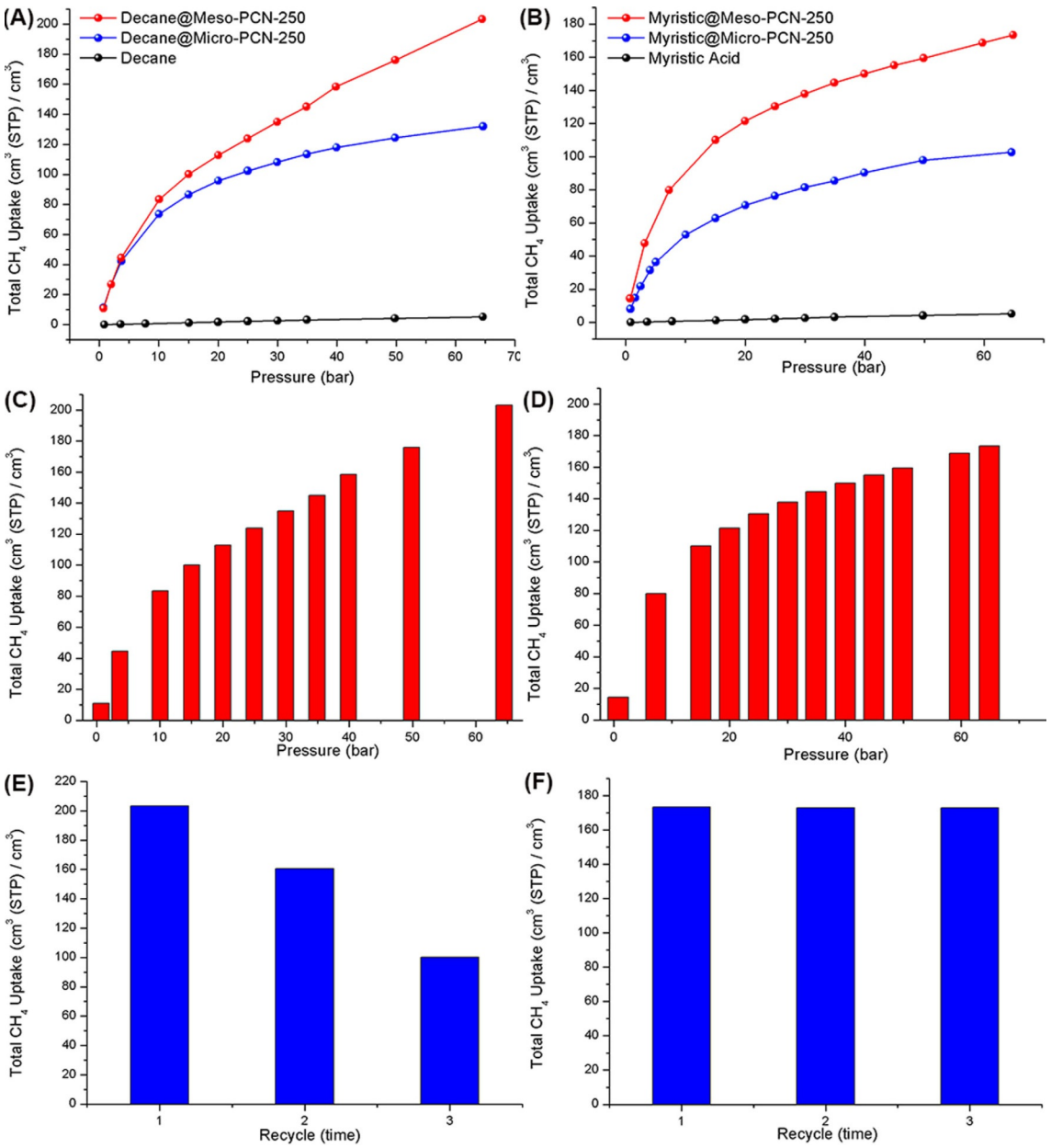

Figure 4. High-pressure methane uptake of Micro-PCN-250 and Meso-PCN-250 doped with n-decane or myristic acid. Volumetric total methane uptake of Micro-PCN-250 and Meso-PCN-250 doped with (A) *n*-decane and (B) myristic acid. Total methane uptake of Meso-PCN-250 doped with (C) *n*-decane and (D) myristic acid at each pressure. Recyclability test of Decane@Meso-PCN-250 doped (E) and Myristic@Meso-PCN-250 (F).

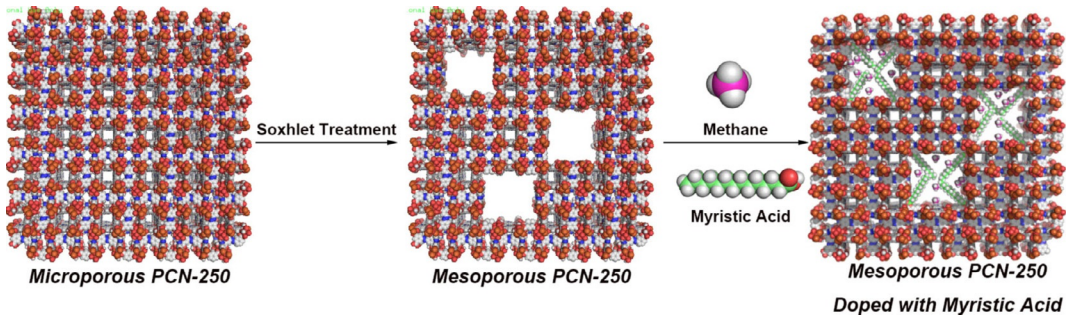

Scheme 1. Schematic illustration of mesoporous PCN-250 doped with myristic acid for enhanced methane uptake.

methods to introduce mesoporous defects in MOFs, it is very rare that a MOF shows increased methane uptake after the treatment.[22] Furthermore, compared to conventional methods previously reported, the HAANG method can produce enhanced methane storage and is more straightforward and more highly recyclable.

In conclusion, we applied a post-synthetic treatment method, termed HAANG, to MOF adsorbents and obtained MOF-hydrocarbon composites with improved methane uptake performance and excellent recyclability. By applying two forms of the same MOF, microporous and mesoporous PCN-250, we observed that doping reagents only improve the methane-uptake performance for Meso-PCN-250 and reduce the performance for Micro-PCN-250. This result indicates that the doping reagents are presumably located within the mesopores or at defect sites in the adsorbent, utilizing the void space and dissolving additional methane molecules. Through doping weakly (*n*-decane) and strongly (myristic acid) binding agents, the Meso-PCN-250 can produce a robust reusable adsorbent composite with increased methane uptake performance. Our findings shed light on the potential for post-synthetic treatment of MOF absorbents to obtain high performing and sustainable natural gas resources.

Acknowledgements

The gas sorption studies were supported by the Center for Gas Separations Relevant to Clean Energy Technologies, an Energy Frontier Research Center funded by the U.S. Department of Energy, Office of Science, Office of Basic Energy Sciences under Award Number DE-SC0001015. The materials were funded by the Robert A. Welch Foundation through a Welch Endowed Chair to H.J.Z. (A-0030) and the National Science Foundation Small Business Innovation Research (NSF-SBIR) under grant no. (1632486). Use of the TAMU Materials Characterization Facility is acknowledged. We also thank framergy, Inc. for providing large reactors and expertise in MOF development. We appreciate the simulation work of Mr. Lan Huang.

Conflict of interest

The authors declare no conflict of interest.

Keywords: high pressure · hydrocarbon · mesoporous · metal–organic framework · methane storage

[1] A. R. Brandt, G. A. Heath, E. A. Kort, F. O'Sullivan, G. Petron, S. M. Jordaan, P. Tans, J. Wilcox, A. M. Gopstein, D. Arent, S. Wofsy, N. J. Brown, R. Bradley, G. D. Stucky, D. Eardley, R. Harriss, *Science* **2014**, *343*, 733 – 735.
[2] V. C. Menon, S. Komarneni, *J. Porous Mater.* **1998**, *5*, 43 – 58.
[3] T. A. Makal, J. R. Li, W. G. Lu, H. C. Zhou, *Chem. Soc. Rev.* **2012**, *41*, 7761 – 7779.
[4] M. Kondo, T. Yoshitomi, K. Seki, H. Matsuzaka, S. Kitagawa, *Angew. Chem. Int. Ed. Engl.* **1997**, *36*, 1725 – 1727; *Angew. Chem.* **1997**, *109*, 1844 – 1846.
[5] J. Fu, Y. Tian, J. Z. Wu, *Adsorption* **2015**, *21*, 499 – 507.
[6] A. Celzard, V. Fierro, *Energy Fuels* **2005**, *19*, 573 – 583.
[7] T. Duren, L. Sarkisov, O. M. Yaghi, R. Q. Snurr, *Langmuir* **2004**, *20*, 2683 – 2689.
[8] S. Q. Ma, D. F. Sun, J. M. Simmons, C. D. Collier, D. Q. Yuan, H. C. Zhou, *J. Am. Chem. Soc.* **2008**, *130*, 1012 – 1016.
[9] Y. Peng, V. Krungleviciute, I. Eryazici, J. T. Hupp, O. K. Farha, T. Yildirim, *J. Am. Chem. Soc.* **2013**, *135*, 11887 – 11894.
[10] J. J. Low, A. I. Benin, P. Jakubczak, J. F. Abrahamian, S. A. Faheem, R. R. Willis, *J. Am. Chem. Soc.* **2009**, *131*, 15834 – 15842.
[11] D. Feng, K. Wang, Z. Wei, Y.-P. Chen, C. M. Simon, R. K. Arvapally, R. L. Martin, M. Bosch, T.-F. Liu, S. Fordham, D. Yuan, M. A. Omary, M. Haranczyk, B. Smit, H.-C. Zhou, *Nat. Commun.* **2014**, *5*, 5723.
[12] W. C. Ikealumba, H. Wu, *Energy Fuels*, **2014**, *28*, 3556 – 3586.
[13] M. H. Arthur, Y. A. Russell, Jr., H. M. Nelly, U. S. Patent, 2,535,148, **1950**.
[14] S. Q. Xia, P. S. Ma, Y. G. Guo, C. Hua, *J. Chem. Eng. Data* **2006**, *51*, 1035 – 1038.
[15] J. M. Ornstein, O. K. Ozdemir, U. S. Patent, 15,112,921, **2016**.
[16] *Detailed description of Soxhlet treatment*, unpublished results.
[17] a) J. Jiang, H. Furukawa, Y.-B. Zhang, O. M. Yaghi, *J. Am. Chem. Soc.* **2016**, *138*, 10244 – 10251; b) C.-C. Liang, Z.-L. Shi, C.-T. He, J. Tan, H.-D. Zhou, H.-L. Zhou, Y. Lee, Y.-B. Zhang, *J. Am. Chem. Soc.* **2017**, *139*, 13300 – 13303.
[18] a) A. Karaipekli, A. Sari, *Renewable Energy* **2008**, *33*, 2599 – 2605; b) T. Kuroiwa, K. Kimura, Y. Aoki, M. A. Neves, S. Sato, S. Mukataka, A. Kanazawa, S. Ichikawa, *J. Food Res.* **2015**, *4*, 133 – 142.
[19] a) S. Yuan, X. Sun, J. Pang, C. Lollar, J.-S. Qin, Z. Perry, E. Joseph, X. Wang, Y. Fang, M. Bosch, D. Sun, D. Liu, H.-C. Zhou, *Joule* **2017**, *1*, 806 – 815; b) A. Kirchon, G. S. Day, Y. Fang, S. Banerjee, O. K. Ozdemir, H.-C. Zhou, *iScience* **2018**, *5*, 30 – 37.
[20] a) K. Vellingiri, J. E. Szulejko, P. Kumar, E. E. Kwon, K.-H. Kim, A. Deep, D. W. Boukhvalov, R. J. C. Brown, *Sci. Rep.* **2016**, *6*, 27813; b) E. A. Vlasova, S. A. Yakimov, E. V. Naidenko, E. V. Kudrik, S. V. Makarov, *Food Chem.* **2016**, *190*, 103 – 109.
[21] A. Kordas, K. Magoulas, S. Stamataki, D. Tassios, *Fluid Phase Equilib.* **1995**, *112*, 33 – 44.
[22] a) K. M. Choi, H. J. Jeon, J. K. Kang, O. M. Yaghi, *J. Am. Chem. Soc.* **2011**, *133*, 11920 – 11923; b) Z. Wang, S. Hu, J. Tang, A. Liang. Y. Li, Q. Zhuang, J. Gu, *Adv. Funct. Mater.* **2018**, *28*, 1707356; c) G. Cai, H.-L. Jiang, *Angew. Chem.* **2017**, *129*, 578 – 582; d) W. Liu, J. Huang, Q. Yang, S. Wang, X. Sun, W. Zhang, J. Liu, F. Huo, *Angew. Chem. Int. Ed.* **2017**, *56*, 5512 – 5516; *Angew. Chem.* **2017**, *129*, 5604 – 5608; e) C. Avci, J. Ariñez-Soriano, A. Carné-Sánchez, V. Guillerm, C. Carbonell, I. Imaz, D. Maspoch, *Angew. Chem. Int. Ed.* **2015**, *54*, 14417 – 14421; *Angew. Chem.* **2015**, *127*, 14625 – 14629; f) S. He, Y. Chen, Z. Zhang, B. Ni, W. He, X. Wang, *Chem. Sci.* **2016**, *7*, 7101 – 7105; g) J. Koo, I. C. Hwang, X. Yu, S. Saha, Y. Kim, K. Kim, *Chem. Sci.* **2017**, *8*, 6799 – 6803.

Manuscript received: August 3, 2018
Accepted manuscript online: September 10, 2018
Version of record online: October 26, 2018